IMPROVED PYROTECHNIC SHOCK SCALING METHOD BASED ON SHOCK RESPONSE SPECTRUM AND STATISTICAL ENERGY ANALYSIS

James Ho-Jin Hwang [(1)], Gerard Borello [(2)], Juan P. Fernandez [(3)]

[(1)] *Jet Propulsion Laboratory, California Institute of Technology, 4800 Oak Grove Drive, Pasadena, CA 91109, USA*
Email: James.Hwang@jpl.nasa.gov
[(2)] *InterAC, 10 Impasse de Bordé Basse, 31240 L'Union, France*
Email: Gerard.Borello@interac.fr
[(3)] *Jet Propulsion Laboratory, California Institute of Technology, 4800 Oak Grove Drive, Pasadena, CA 91109, USA*
Email: Juan.P.Fernandez@jpl.nasa.gov

ABSTRACT

It has been more than forty years since the pyrotechnic shock scaling method was introduced. The scaling method estimates the attenuation of the Shock Response Spectrum (SRS) based on the distance from the source, structural configurations, types of structural joints and interfaces, and intervening structure [1]. The method has been successfully used in the spacecraft community countless times and still is frequently used to develop pyrotechnic shock requirements at various levels of assembly of a spacecraft. However, since the method was derived empirically from a limited set of shock test data [2], the aerospace community has been looking for an alternative approach. In this paper, a computational scaling method based on Statistical Energy Analysis (SEA) is re-visited. SEA is traditionally used as a method for investigating the diffusion of acoustic and vibratory energies of a system at steady-state [3]. Previously, an approach using the SRS as an acceleration constraint condition to the SEA model was introduced to estimate the attenuation from a shock source [4,5]. In the current investigation, additional examples are provided to further validate the approach. In addition, responses in the time domain are produced by the Local Modal Phase Reconstruction (LMPR) approach which was recently introduced to the community [6].

1. INTRODUCTION

In modern spacecraft engineering, where the design and modelling are largely based on computer-aided tools, pyrotechnic shock analyses are still frequently carried out by empirical methods. Especially, sub-system level pyrotechnic shock requirements of a spacecraft are often produced by the scaling method [1]. Based on testing experience and empirical rules that were established more than forty years ago, the scaling method estimates the attenuation of a shock due to distance, structural configurations, types of joints and interface, and intervening structure [1]. While the method was developed with a limited set of data to provide a first-cut estimate, it is nonetheless frequently used as a standard tool in spacecraft design; as a result, inaccuracy and inefficiency of the approach have been widely experienced and reported in the community [7].

In numerical simulations, pyrotechnic shock modelling is typically considered as a transient Finite Element (FE) problem with the implicit or explicit time iteration scheme and the modal transient on occasion [6]. The Finite Element (FE)-based direct time integration methods could produce accurate results; however, especially in large-scale system level modelling, engineers frequently face the following challenges; 1. As the frequency increases, system responses produce high modal overlap and high modal density; it could be difficult to develop a FE model that is valid in the frequency range of pyrotechnic shock environment, 2. Since at least six or more elements are typically used per wavelength in the transient FE modelling, the size of a high fidelity system model that is valid in the frequency range of pyrotechnic shock environment could be enormous and may pose a computational challenge, 3. Inherent numerical stability issues. In addition, as the duration of the shock pulse is less than a few milliseconds with the magnitudes changing drastically within that time frame, extremely short time steps required for the computation could further complicate the simulation, 4. The governing equations of motion require shock input forcing functions that are difficult to measure and are not readily available in the shock testing community.

Alternatively, this paper investigates pyrotechnic shock modelling using Statistical Energy Analysis (SEA). Unlike FE-based transient methods, SEA produces dynamic responses as ensemble averages in the frequency domain. A typical SEA model is comprised of structural and acoustic subsystems that are primarily defined by geometric and material attributes of the system plus wave-bearing characteristics. The subsystems are connected by junctions which are defined by the coupling loss factor (CLF). The CLF describes the power flow that is proportional to the difference in energy levels among subsystems and is obtained by the wave equations and geometric boundary conditions such as Snell's law of refraction. As the method is statistical, a high number of modes and overlap are essential to produce accurate results; the SEA method is frequently used in system level vibration and acoustic modelling.

2. SHOCK MODELLING USING SEA

Since the statistical nature of the method allows SEA to be an appropriate modelling tool in the frequency range

This research was carried out at the Jet Propulsion Laboratory, California Institute of Technology, under a contract with the National Aeronautics and Space Administration. © 2018. All rights reserved.

where the modal density and modal overlap are high, researchers have shown interest in applying the method to pyrotechnic shock simulation. There are primarily two types of SEA-based approaches available in the literature. The transient SEA method is based on the following first order differential equation for an isolated system,

$$P(t) - \frac{\partial E}{\partial t} = \eta_{tot}\omega E \tag{1}$$

in which *P(t)* is power, *E(t)* is energy, η_{tot} is the damping loss factor, and ω is angular frequency. The energy *E(t)* as an instantaneous value is,

$$\overline{E(t,\Delta T)} = \frac{m}{\Delta T}\int V(t,\tau)^2 d\tau \tag{2}$$

in which *m* is mass and $V(t, \tau)^2$ is the auto-spectrum of the instantaneous velocity. Since there is a slow time evolution of the auto-spectrum of diffuse resonant energy, injected power *P(t)* is also expected to vary slowly in accordance to ΔT. Time solutions of the transient SEA method are then time decaying exponential functions as found in the reverberation time of a system. Since these solutions are not fast enough, researchers have not been able to apply the transient SEA method successfully to pyrotechnic shock applications. Manning and Lee [8] used steady-state CLF instead of the transient CLF. Lai and Soom [9,10] investigated convergence of the transient CLF at each time step and proposed an alternative transient SEA formulation that could utilize the steady-state CLF. In terms of complete transient SEA solutions, simple resonators and beam models subjected to an impulse-like function were developed by Pinnington and Lednik [11,12].

The second method, which is also the basis of the proposed approach, utilizes the traditional steady-state SEA modelling to produce system frequency response function (FRF) and transfer function (TF) that are valid in the frequency range of pyrotechnic shock environments. Solutions in the time domain are obtained by a synthesis of the response in the frequency domain. In the past, a method named Virtual Mode Synthesis Simulation (VMSS) was proposed [13,14]. In short, the VMSS assumes dynamic modes are distributed over a frequency band of interest according to the estimated modal density and the modes produce the frequency response envelope collectively at each resonant frequency. FRF magnitude of the virtual system is matched with that of the SEA model by curve fitting. In this investigation, the Local Modal Phase Reconstruction (LMPR) method, which is simpler and more physically realistic, is used to produce a time synthesis.

2.1 Shock Scaling Based on SEA Modelling

At the heart of the computational scaling method is the FRF and TF developed from a SEA model. For a linear time invariant system, an input signal *x(t)* with Fourier transform *X(f)* passes into system transfer function *H(f)* to yield an output with Fourier transform *Y(f)*, such as in Fig. 1.

$$Y(f) = H(f)X(f) \tag{3}$$

Figure 1. Transfer Function H(f)

Transfer function *H(f)* could be described as a prediction of the real-valued transfer velocity between a source and a receiver subsystem in the selected analysis bandwidth *B* and its central frequency f_c,

$$H(f_c, B) = \left|\frac{V_r}{V_s}\right| = \sqrt{\frac{m_s E_r}{m_r E_s}} \tag{4}$$

in which *V* is velocity, subscript *s* is source, and subscript *r* is receiver. For the proposed shock scaling, the Shock Response Spectrum (SRS) is used in lieu of the Fourier transform *X(f)* as a complete representation of the input time signal in the frequency domain,

$$SRS_r(f) = H(f)SRS_s(f) \tag{5}$$

Since the shock scaling method is based on the attenuation of the SRS in the frequency domain, Eq. 5 is sufficient to produce the desired results. In addition, time histories could be synthesised from the SRS based on the LMPR methodology.

2.2 LMPR Time Synthesis

The LMPR methodology estimates time histories for a receiver subsystem from the SEA transfer function *H(f)* in the following steps. First, velocity of a receiver subsystem is estimated as follows,

$$U(x,\omega) = \sum_n \frac{j\omega F_n}{{\omega_n}^2 - \omega^2 + j\eta_n\omega\omega_n} \tag{6}$$

in which *x* is a position within the receiver subsystem and the force F_n is calculated by a Dirac delta applied at a receiver boundary. Second, the TF of the LMPR algorithm (complex gain *GU*) is obtained by interpolation and integration of the SEA *H(f)* modulus within the band of interest and the prescribed velocity.

$$\langle G\rangle = \frac{1}{df}\int \frac{H(f_c,\Delta f)}{|U|} df \tag{7}$$

$$H_{LMPR}(f) = \langle G\rangle U \tag{8}$$

Third, phase terms that will be oscillating around the wavenumber of the receiver subsystem are produced,

$$H_{LMPR}(f) = |H(f)|\langle e^{j\phi(f)}\rangle \qquad (9)$$

in which, $\phi(f)$ is the reconstructed phase of the local mode. Finally, a synthesized time history is produced with a general function in the time domain which is a part of convolution integral,

$$x(t) = FFT^{-1}\{H_{LMPR}(f)\}s(t-\delta) \qquad (10)$$

in which $x(t)$ is the synthesized time history and $s(t\text{-}\delta)$ is a general function in the time domain with a lag.

3. NUMERICAL EXAMPLES

The traditional scaling method estimates the attenuation of the SRS in two regions; the attenuation of the low frequency (below the knee frequency) constant velocity line and the attenuation of the high frequency (beyond the knee frequency) peak accelerations as a function of distance from the source. Ref. [1] suggests that the attenuation of the constant velocity line was roughly the same for all types of structures; however, the attenuation of the high frequency peak shock response was different for various structural types. Fig. 2 shows the attenuation of the constant velocity portion of the SRS as a function of distance and Fig. 3 shows the attenuation of the peak SRS level as a function of distance for various structural configurations. Examples from two case studies are provided.

3.1 Cylinder Model

The first example is of a cylinder model as shown in Fig. 4. The model is comprised of nine cylinder subsystems. Each subsystem is modelled with simply supported boundary conditions, 0.5*m* in length, 0.5*m* in radius, and 10*mm* thickness. The subsystems are made out of aluminium (42.41*kg* each) and connected by line junctions with 180-degree panel angle. It is assumed that the first subsystem is constrained as the source with 1*g* SRS from 16Hz to 10000Hz. The input energy was assumed to produce bending waves from the receiver subsystems; no shear or extensional waves were incorporated. The total length of the receiver subsystems was 4*m* (157.48*in*) and a constant 5% damping loss factor (η) was used across the model. Modal density of each subsystem shows that at least one mode is available starting at 500Hz indicating that is the lowest valid frequency of the model. With the SRS as the energy constraint condition, response of each subsystem was scaled by the input in the frequency domain. Fig. 5 shows the comparison between the SEA prediction and the attenuation of constant velocity line in Fig. 2. For the comparison, results from the SEA model were arithmetically averaged to estimate the attenuation from 500Hz to 1000Hz. Fig. 6 shows the comparison between the SEA prediction and the cylindrical shell attenuation curve in Fig. 3. The SEA results from 1000Hz to 10000Hz were arithmetically averaged in order to provide a comparison to the curve in Fig. 3. The computational scaling method based on the SEA modelling generated promising results; in both cases, the method predicted attenuation that was very close to those in Figs. 2 and 3. Fig. 6 appears to show one of the key assumptions in successful SEA modelling, *i. e.*, high modal density and high modal overlap. As the first bending mode is around 500Hz and the number of modes exceeds three at 1000Hz, fidelity of the model would be more appropriate for the prediction of peak shock response attenuation. However, both results clearly demonstrate the effectiveness of the new approach.

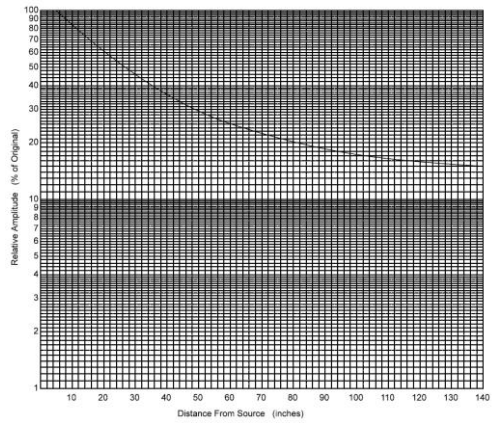

Figure 2. Attenuation of Constant Velocity Line [1]

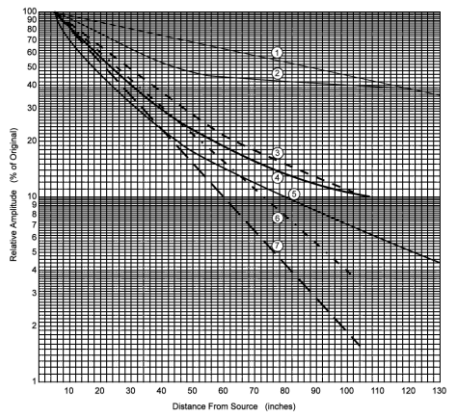

Figure 3. Peak Pyrotechnic Shock Response vs Distance (1. Honeycomb structure, 2. Longeron or stringer of skin/ring-frame structure, 3. Primary truss members, 4. Cylindrical shell, 5. Ring frame of skin/ring-frame structure, 6. Complex equipment mounting structure, 7. Complex airframe) [1]

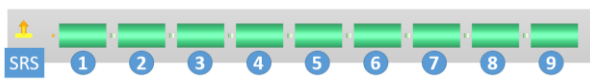

Figure 4. SEA Cylinder Model

3.2 Composite Panel Model

The second example is of a 0.46*m* (18*in*) by 1.22*m* (48*in*) composite panel model as shown in Fig. 7. The panel is made of 25.40*mm* (1*in*) thick foam core (1000*kg/m*^{3} density) and 1*mm* thick carbon fiber graphite face sheets, plus one aluminium plate hosting a 15.88*mm* (5/8*in*) cable cutter. Total weight of the composite panel was 15.84*kg* and the weight of the aluminium plate was

0.40*kg* including the cable cutter. Fig. 8 shows the SEA model representing the test setup. A ball peen hammer was used to impart a shock onto the panel by sharply striking the base aluminium plate. Accelerometer measurements taken near the impact point (Location 1) served as the shock source data. Also, shock measurements were made at two other panel locations, one approximately 12*in* away (Location 2), and the other 24*in* away (Location 3) from the shock source. A National Instruments PXI chassis with 200K sample rate and PCB 350D02 shock accelerometers were used to acquire the test data.

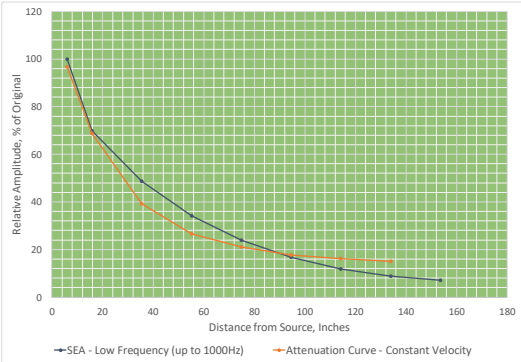

Figure 5. Comparison between SEA Prediction at Low Frequency and Constant Velocity Line Attenuation

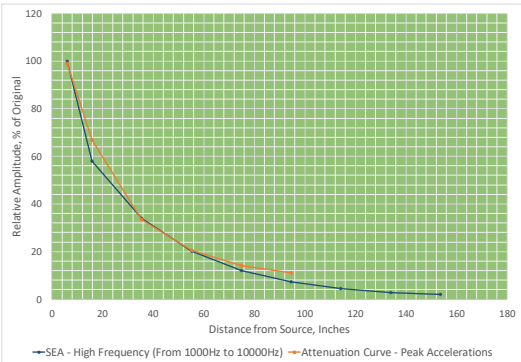

Figure 6. Comparison between SEA Prediction at High Frequency and Cylindrical Shell Attenuation

The SEA model (Fig. 8) is comprised of six sandwich panel subsystems and one aluminium plate subsystem. The subsystems are connected by line junctions with a 180-degree panel angle, except for the aluminium plate subsystem which was modelled by four point connections with the subsystem underneath. It was assumed that the source energy would induce all wave components (bending, shear, and extensional) of the panel; this was necessary because, unlike the cylinder, shear and extensional wave components play a major role in panel response due to their relatively high modal densities in the frequency range of interest. Finally, a constant 1% damping loss factor (η) was assumed for the aluminium subsystem and a 0.3% to 3.0% damping loss factor (η) for the composite panel. Since the aluminium plate is only to provide the shock input, damping of the plate does not play a significant role in panel response. Fig. 9 shows the estimated damping loss factor of the composite panel based on best estimate.

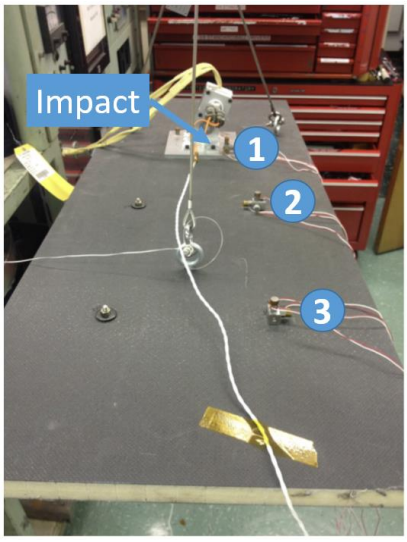

Figure 7. Panel Shock Test Setup

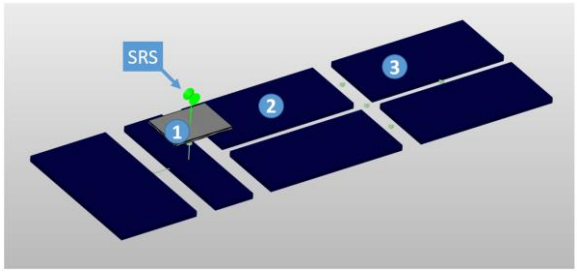

Figure 8. SEA Model of Panel Shock Testing

The following steps were taken to estimate attenuation across the SEA model. First, accelerations that were measured at the base of the aluminium plate (Location 1) were converted to SRS with Q=10. Second, only the maximum value was taken among the X, Y, and Z SRS components at each frequency to produce the max SRS (Fig. 10). Third, the max SRS was imposed as the energy constraint condition at Location 1 (aluminium plate subsystem). Finally, responses were recovered from the receiver subsystems to estimate attenuation at Location 2 and Location 3.

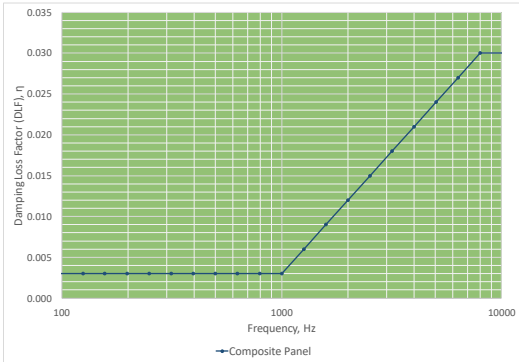

Figure 9. Estimated Damping Loss Factor (DLF) of Composite Panel

Figure 11 shows the comparison among the predicted

SRS response at Location 2, result from the traditional scaling, and the measured test data. Only the maximum value of the X, Y, and Z acceleration components was taken from the test data at each frequency for comparison. This was necessary because not only was the max SRS used as input, the SEA model produces results in bending, shear, and extensional directions that are not in the same coordinates as the measured test data.

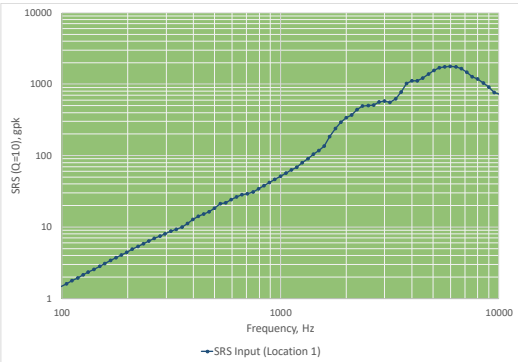

Figure 10. Input SRS Constrained at Location 1

The SEA model shows the first mode around 500Hz, which indicates the lowest valid frequency of the model. The empirical scaling method was applied to the input shock curve from Fig. 10 based on the constant velocity line attenuation in Fig. 2 and the peak shock attenuation curve for Honeycomb structure in Fig. 3. In addition, 50% additional knockdown was applied to the peak accelerations region to simulate the attenuation due to the joint between the aluminum plate and the composite panel. Overall, the proposed method predicted attenuation that matched well with the test data. The empirical scaling method produced a large disparity above 1000Hz but did better below 1000Hz. The over-prediction may be due to, in part, the use of Honeycomb structure attenuation curve as no empirical attenuation curve is available for a foam panel. Since the traditional scaling method is purely empirical without rigorous mathematical justification, the results should be used with care. Fig. 12 shows the comparison at Location 3. Similar observations can be made; the new computational scaling method based on the SEA modelling predicted attenuation that closely matched the test data. The empirical scaling method over-predicted attenuation at high frequency; while it did better below 1000Hz.

Finally, the LMPR algorithm was utilized to produce the synthesized time histories at two locations. Fig. 13 shows the comparison between the measured time history in the Z axis and the synthesized time history of the bending response at Location 2. Fig. 14 shows the comparison at Location 3, this time with the response in the Y axis and the synthesized bending response. In both cases, the LMPR method produced time histories that were in close agreement with the test data; decay of the time history and the maximum acceleration magnitude appear reasonable.

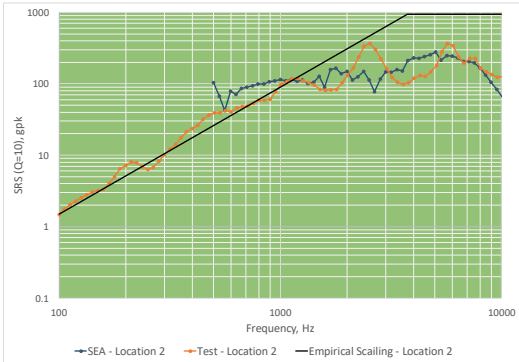

Figure 11. Comparison of SEA, Traditional Scaling, and Test Data (Location 2)

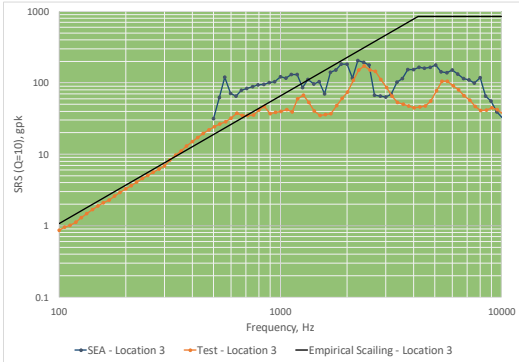

Figure 12. Comparison of SEA, Traditional Scaling, and Test Data (Location 3)

4. CONCLUSIONS AND RECOMMENDATIONS

The new computational scaling method based on SEA modelling produced reasonable results in two case studies. The method is based on the FRF and TF of a linear time invariant system model. While the method is based on rigorous mathematical principles, limitations and constraints of the SEA theory still apply such as high modal density and high modal overlap assumptions. As a result, the method is well-suited for system level modelling such as development of pyrotechnic test and analysis requirements at various levels of assembly of a spacecraft. The proposed method could be further advanced by incorporating a FE-based FRF and TF-type approach to improve the low frequency prediction capability.

5. REFERENCES

1. NASA Goddard Space Flight Center. (2013). General Environmental Verification Standard (GEVS) For GSFC Flight Programs and Projects, GSFC-STD-7000A, NASA Goddard Space Flight Center, Greenbelt, Maryland.

2. Kacena-III, W.J., McGrath, M.B. & Rader, W.P. (1970). Aerospace Systems Pyrotechnic Shock Data, NASA Contractor Report-116437, -116450, -116401, -116402, -116403, -116406, and -116019, Vol. I-VII, Goddard Space Flight Center, Greenbelt, Maryland.

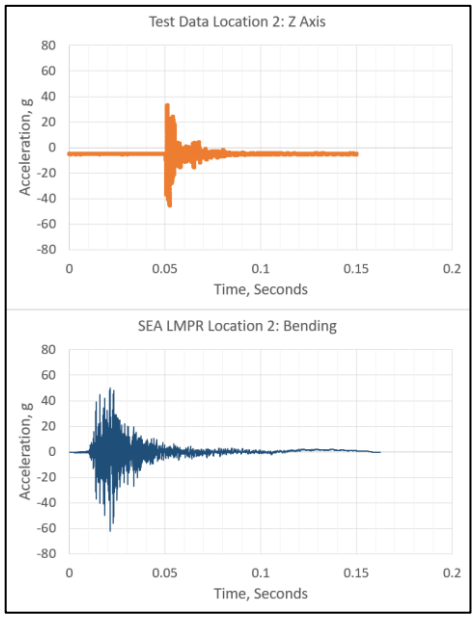

Figure 13. Time History Comparison between Test Data and LMPR Synthesis (Location 2)

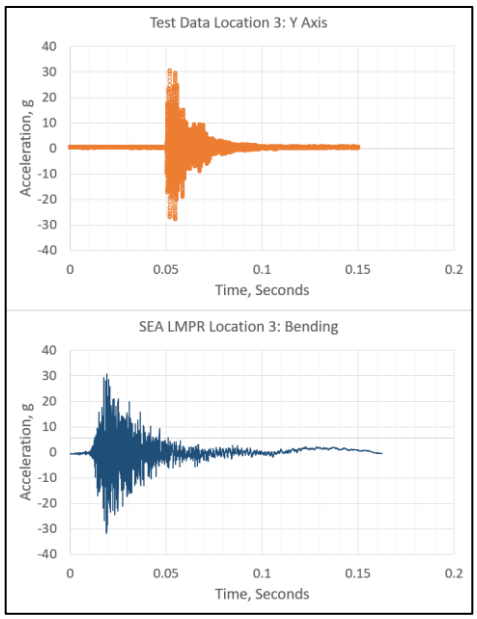

Figure 14. Time History Comparison between Test Data and LMPR Synthesis (Location 3)

3. Lyon, R.H. & DeJong, R.G. (1995). *Theory and Application of Statistical Energy Analysis (Second Edition)*, Butterworth-Heinemann, Newton, MA.

4. Hwang, J.H-J., MacLeod, B. & Palestine, E. (2015). High Fidelity Response Simulation Due to Shock Response Spectrum Using Statistical Energy Analysis. In. Proc. 2015 Spacecraft and Launch Vehicle Dynamic Environments Workshop, Online at http://www.aerospace.org/education/conferenceproceedings/2015-sclv-proceedings/ (as of 26 April 2018), Aerospace Corporation, El Segundo, CA.

5. Hwang, J.H-J. & Altmann, C. (2016). Pyrotechnic Shock Scaling Method Based on Shock Response Spectrum and Statistical Energy Analysis. In Proc. 14th European Conference on Spacecraft Structures, Materials & Environmental Testing, Online at http://ecssmet2016.com/abstract/index.php?onglet=7 (as of 26 April 2018), INSIGHT OUTSIDE, Meylan, France.

6. European Cooperation for Space Standardization (ECSS). (2015). Space engineering: Mechanical shock design and verification handbook, ECSS-E-HB-32-25A, ECSS Secretariat, ESA-ESTEC, Requirements & Standards Division, Noordwijk, The Netherlands.

7. Hardt, A. (2017). Shock Attenuation vs. Distance for a Cylindrical Shell. In. Proc. 2017 Spacecraft and Launch Vehicle Dynamic Environments Workshop, Online at http://www.aerospace.org/education/conferenceproceedings/2017-sclv-proceedings/ (as of 26 April 2018), Aerospace Corporation, El Segundo, CA.

8. Manning, J.E. & Lee, K. (1968). Predicting Mechanical Shock Transmission. Shock and Vibration Bulletin, No. 37, Pt. 4, pp. 65-70.

9. Lai, M.L. & Soom, A. (1990). Prediction of Transient Vibration Envelops Using Statistical Energy Analysis Techniques. *J. Vib. Acoust* **112**(1), 127-137.

10. Lai, M.L. & Soom, A. (1990). Statistical Energy Analysis for the Time-Integrated Transient Response of Vibrating Systems. *J. Vib. Acoust* **112**(2), 206-213.

11. Pinnington, R.J. & Lednik, D. (1996). Transient Statistical Energy Analysis of an Impulsively Excited Two Oscillator System. *Journal of Sound and Vibration* **189**(2), 249-264.

12. Pinnington, R.J. & Lednik, D. (1996). Transient Energy Flow Between Two Coupled Beams. *Journal of Sound and Vibration* **189**(2), 265-287.

13. Dalton, E.C. (1999). High Frequency Shock Prediction Short Course, Military Technology, Inc., Huntsville, AL.

14. Loper, B. Frydman, A. Berman. M. & Li, D. (2000). Validation of Ballistic Shock Prediction Models and Techniques for Use in the Crusader Combat Vehicle Program. 11th Annual US Army Ground Vehicle Survivability Symposium.